FREQUENCY OF DUST STORMS IN THE WESTERN ARCADIA PLANITIA: COMPARISON WITH REANALYSIS DATA

K. Ogohara, *Faculty of Science, Kyoto Sangyo University, Kyoto, Japan (ogohara@cc.kyoto-su.ac.jp)*

Introduction:

The Arcadia Planitia (Fig. 1) is one of the most outstanding dust storm zones in the northern mid-latitudes on Mars. Wang, Zurek, & Richardson (2005) and Guzewich et al. (2015) showed that the northern mid-latitude dust storms tended to occur in three regions, the Acidalia, the Arcadia, and Utopia. Kulowski, Wang, & Toigo (2017) reported that most of dust storms observed in the three regions were categorized into "plume-like dust storm", which is apparently different from dust storms that tend to be observed in the low-latitudes and the southern mid-latitudes. Mars. Wang, Zurek, & Richardson (2005) additionally revealed that the dust storm frequency got lower near the northern winter solstice in the regions and was associated with the eddy activity in the northern mid-latitudes. The eddy activity they mentioned means the baroclinic instability and the associated frontal system. Although I agree with their suggestion, a correlation between dust storm initiations and the phase of the baroclinic eddies is a key to understand the initiation mechanisms of the dust storms if the baroclinic eddies contribute to initiations of the dust storms. That is whether dust storms tend to break out in the trough, ridge, or boundary between them. In this study, the phase of the baroclinic waves suitable for dust storm initiations in the northern mid-latitudes are investigated.

Data and method:

I used reflectance data from red and blue bands (575–675 nm and 400–450 nm, respectively) images acquired by Mars Orbiter Camera onboard Mars Global Surveyor (MGS/MOC), limiting our investigation to the region centered around 180°E−40°N (the west of the Arcadia Planitia, WAP). We examined 800 × 600-pixel (40◦ × 30◦) subsets of the full size MOC wide angle camera (MOC-WA) image swathes. The subsets are centered at 180◦E− 40◦N and were extracted from the MOC-WA images taken outside the global dust storm period in Mars Year (MY) 25. Fig. 2 shows four examples of MOC red images including dust storms. Dust storms in the western Arcadia Planitia were listed based on the automated segmentation algorithm for Martian dust storms developed by Ogohara & Gichu (2022). After the automated detection of dust storms, false positives were removed by visually inspecting all the detection results. The three-dimensional distributions of the atmospheric temperature, zonal wind, meridional wind, geopotential height, surface pressure, and the surface stress at the initiation date of the dust storms are based on the background data (short-term forecast from analysis) included in the Ensemble Mars Atmosphere Reanalysis System (EMARS) (Greybush et al., 2019). The variables on a few pressure levels were interpolated from the original vertical coordinate, the hybrid coordinate of σ-p.

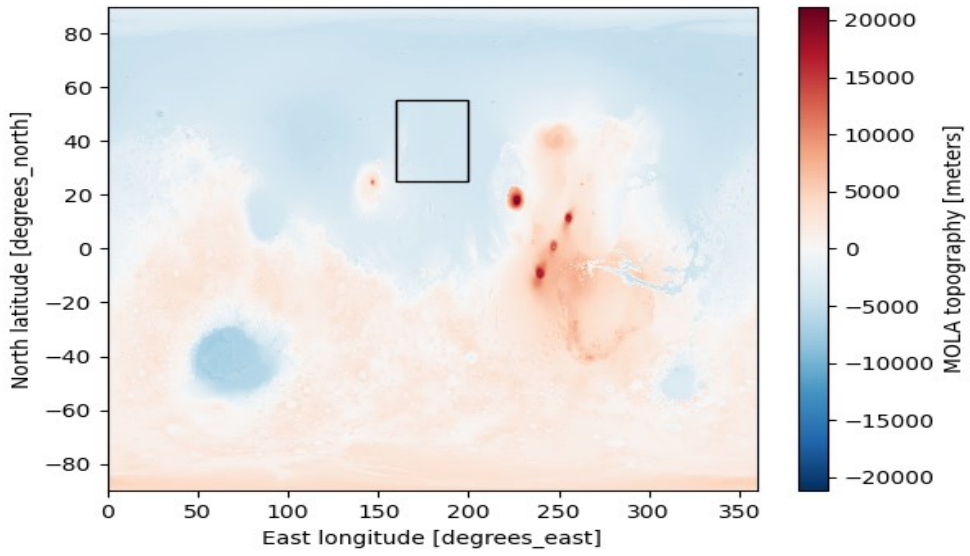

Figure 1 Mars topography distributed through Mars Climate Database 5.0. A black rectangle indicates the target region, the western Arcadia Planitia.

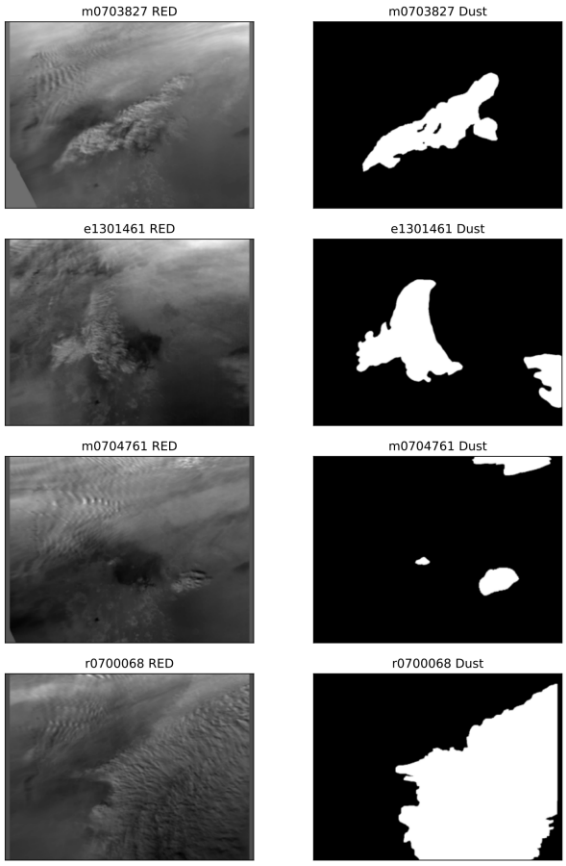

Figure 2 Examples of (left) MOC red images including dust storms and (right) areas covered by dust storms. White areas in the right column are dust storms determined subjectively by the author.

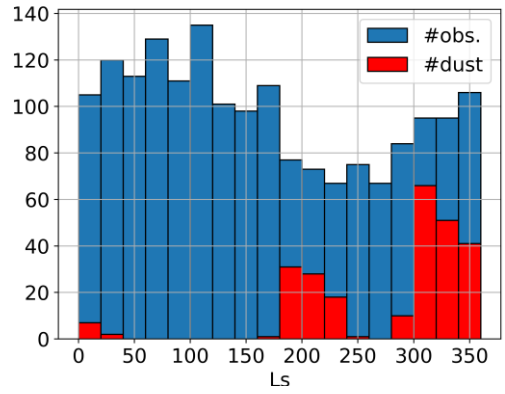

Figure 3 The seasonal variability of dust storm frequency in WAP observed by MGS/MOC in MYs 24, 26, and 27. The Blue bars indicate the total number of images, and the red bars indicate the number of images capturing dust storms.

Dust storm frequency in WAP: Fig. 3 shows the seasonal variation of dust storm frequency in WAP and is consistent with Wang, Zurek, & Richardson (2005). During the northern mid-winter season, dust storm activity in WAP temporally decreases. In contrast, the seasons before and after that season show high dust storm frequency. As Wang, Zurek, & Richardson (2005), such seasonal variability of dust storm frequency in WAP is reminiscent of the relationship with the activity of baroclinic waves in the mid-latitudes, which also paused in the northern mid-winter (Lee, Richardson, Newman, & Mischna, 2018; Lewis et al., 2016).

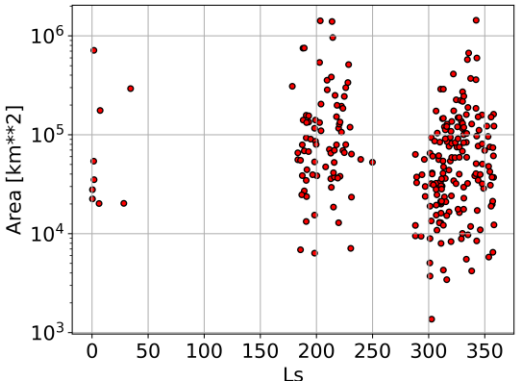

Figure 4 The seasonal variability of dust storm area in km^2.

Fig. 4 shows the seasonal variability of dust storm size in km^2. Some regional dust storms, which were defined as events larger than 1.6 x 10^6 km^2 by (Cantor, James, Caplinger, & Wolff, 2001) were detected in this study. Area of the regional dust storms was underestimated because they were trimmed by the edges of the image subsets. The mean sizes of dust storms are not largely different between the seasons before and after the northern winter solstice.

Relationship with the synoptic scale phenomena: By extracting from EMARS the three-dimensional distributions of several variables (e.g., temperature, wind) at the date and time closest to the dust storm observation time and calculating their time averages, a typical synoptic scale atmospheric state at the initiations of the dust storms can be derived. Your abstract should not be more than 4 pages long. Fig. 5 demonstrates the composite means of zonal wind, meridional wind, the surface pressure, and the surface stress anomalies from the zonal means during the season from the northern late winter in MY24 to the next northern spring equinox. Anomalies in zonal and meridional winds shown in the figure are derived on the 3 hPa pressure level. WAP is located at the center of each panel of the figure. The low frequency components and the diurnal tides were attenuated in advance by the running means at each grid point with the full widths of one month and one sol, respectively.

It is easily found in Fig. 5 that, at the dust storm

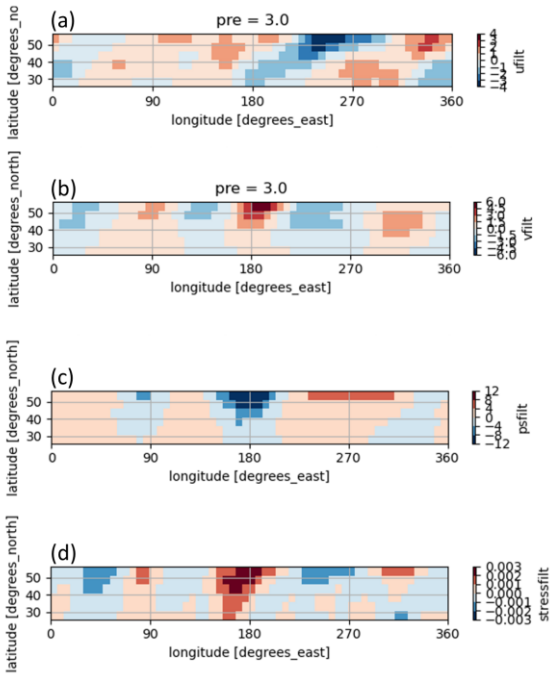

Figure 5 The composite means of (a) zonal wind, (b) meridional wind, (c) the surface pressure, and (d) the surface stress anomalies at the dates and times of the dust storm initiations.

initiations, WAP tends to be in the southerly wind and low-pressure phase of the baroclinic waves. Area with negative anomaly in zonal wind is elongated from the northeast to the southwest. The surface stress tends to be high especially in the northern part of WAP. In any case, it can be seen that dust storms in the WAP tend to occur at the southern end of the latitudinal range where the baroclinic eddies are active.

Discussions and conclusions: Fig. 5 seems to imply the synoptic scale atmospheric conditions typical to the dates and time of the dust storm initiations. However, considering that the typical period of the baroclinic waves is a few sols on Mars, Fig. 5 may contain non-negligible uncertainty. It is widely known that MGS could observe WAP only once every sol, ~14LT. All of dust storms investigated in this study were recorded as if they all broke out around 14LT. This means that there is an uncertainty of one sol in the onset time of the dust storms, and if the period of the baroclinic waves is two sols, this corresponds to an uncertainty of half a wavelength. Then, dust storms in WAP are not necessarily more likely to occur in the low-pressure and southerly wind phase. More frequent observations are needed to better clarify the relationship between dust storm onsets and the phase of the baroclinic waves. In addition, it is necessary to verify that reanalysis data is reliable so that it can be used for such studies, for example, by trying to use the analysis data instead of the background data or by investigating ensemble spreads.

References:

Cantor, B. A., James, P. B., Caplinger, M., & Wolff, M. J. (2001). Martian dust storms: 1999 Mars Orbiter Camera observations. *Journal of Geophysical Research*, *106*(E10), 23653–23687.

Greybush, S. J., Kalnay, E., Wilson, R. J., Hoffman, R. N., Nehrkorn, T., Leidner, M., … Miyoshi, T. (2019). The Ensemble Mars Atmosphere Reanalysis System (EMARS) Version 1.0. *Geoscience Data Journal*, *6*(2), 137–150. https://doi.org/10.1002/gdj3.77

Guzewich, S. D., Toigo, A. D., Kulowski, L., & Wang, H. (2015). Mars Orbiter Camera climatology of textured dust storms. *Icarus*, *258*, 1–13. https://doi.org/10.1016/j.icarus.2015.06.023

Kulowski, L., Wang, H., & Toigo, A. D. (2017). The seasonal and spatial distribution of textured dust storms observed by Mars Global Surveyor Mars Orbiter Camera. *Advances in Space Research*, *59*(2), 715–721. https://doi.org/10.1016/j.asr.2016.10.028

Lee, C., Richardson, M. I., Newman, C. E., & Mischna, M. A. (2018). The sensitivity of solsticial pauses to atmospheric ice and dust in the MarsWRF General Circulation Model. *Icarus*, *311*, 23–34. https://doi.org/10.1016/j.icarus.2018.03.019

Lewis, S. R., Mulholland, D. P., Read, P. L., Montabone, L., Wilson, R. J., & Smith, M. D. (2016). The solsticial pause on Mars: 1. A planetary wave reanalysis. *Icarus*, *264*, 456–464. https://doi.org/10.1016/j.icarus.2015.08.039

Ogohara, K., & Gichu, R. (2022). Automated segmentation of textured dust storms on mars remote sensing images using an encoder-decoder type convolutional neural network. *Computers and Geosciences*, *160*(June 2021), 105043. https://doi.org/10.1016/j.cageo.2022.105043

Wang, H., Zurek, R. W., & Richardson, M. I. (2005). Relationship between frontal dust storms and transient eddy activity in the northern hemisphere of Mars as observed by Mars Global Surveyor. *Journal of Geophysical Research*, *110*(E7), 1–20. https://doi.org/10.1029/2005JE002423